Development of optimal models of porous media by combining static and dynamic data: The porosity distribution

Hossein Hamzehpour[1] and Muhammad Sahimi[2,*]

[1]*Institute for Advanced Studies in Basic Sciences, Gava Zang, Zanjan 45195-1159, Iran*

[2]*Mork Family Department of Chemical Engineering & Materials Science, University of Southern California, Los Angeles, California 90089-1211, USA*

This paper is part of a project, the goal of which is the development of the optimal spatial distributions of the porosity and permeability of a large-scale porous medium by using complementary static and dynamic data for the medium. The data include limited measurements of the porosity, which the method honors (preserves) in the optimal model and utilizes its correlation function, together with the first-arrival (FA) times, at a certain number of receivers, of seismic waves that have propagated in the medium and the time dependence of the pressure of a fluid flowing in the medium. The method uses the simulated-annealing (SA) technique in order to develop the optimal model. In the present paper we utilize the porosity and FA times data in order to develop the optimal spatial distribution of the porosity. This is accomplished by combining the SA method with a simulator that solves for the numerical solution of the acoustic-wave equation from which the FA times are estimated, limited porosity, and FA times data. We show that the optimal model not only honors the data, but also provides accurate estimates of the porosities in the rest of the porous medium. The efficiency of the computations is discussed in detail.

PACS number(s): 47.56.+r, 05.90.+m, 05.40.−a

I. INTRODUCTION

Due to their practical importance and large number of applications, the development of accurate models of porous materials [1,2] and other types of heterogeneous media [3,4] has been the subject of numerous studies over the past several decades. In particular, *reconstruction* of such disordered media, i.e., development of models for them based on a limited amount of experimental data for some of their properties, has been investigated by many research groups [5–12]. Most of the methods that were developed by these groups [5–11] were based on information that represents one-point (volume fraction) and two-point correlation functions. Torquato and co-workers [12–14] suggested another method, a variation of the simulated annealing (SA) technique [15], which can, in principle, be used with any type and number of correlation functions. Their method is, in effect, one of optimization, i.e., one by which a limited amount of data for a given system is utilized and the SA technique is used to develop the optimal model that satisfies the constraints that the data impose on the optimization problem. Torquato and co-workers used the method for reconstructing a variety of porous and composite materials. In particular, they used the method [14] to reconstruct laboratory-scale samples of Berea and Fontainebleau sandstones, which are important to the understanding of fluid flow and transport in oil reservoirs and groundwater aquifers.

The above works focused on reconstructing and modeling of *laboratory-scale* porous media. The focus of the present paper is on the development of optimal models of large-scale (LS) porous media, those that are much larger than laboratory-scale porous materials considered previously. Examples include oil, gas, and geothermal reservoirs, and groundwater aquifers. However, as we explain below, the method is equally applicable to laboratory-scale porous media. Such porous formations are very heterogeneous, with the heterogeneities manifesting themselves as broad spatial distributions of the porosity and permeability, and the anisotropy caused by stratification (layering) of the formations. To model LS porous media by any method, one must first analyze the various types of data that are typically available, which may be divided into two important groups.

(1) In one group are what we call the *direct* data. Two important properties of LS porous media, namely, the distributions of their porosity ϕ and permeability k, belong to this group. The porosity is estimated routinely along, for example, wells during their drilling, or evaluated relatively accurately by indirect methods, such as measuring the resistivity of samples of the porous medium, and also through seismic data (see below). The permeabilities can be estimated by *in situ* nuclear-magnetic resonance [16] which is, however, costly as one must make a very large number of measurements. They can also be measured by coring and laboratory measurements, which may not be very accurate because the state of a sample porous medium at a certain depth in a natural formation may be quite different from its state in a laboratory. Alternatively, very useful information about the permeabilities' spatial distribution is obtained through analysis of the time dependence of the pressures or fluxes of fluids at, for example, certain points in the porous medium where the fluids are produced (e.g., production wells in an oil reservoir). Such data are routinely recorded and their amount is typically very extensive. Assuming that the structure of a porous medium does not change much over time scales on the order of months or a few years, the porosity and permeability data represent *static* information.

(2) In the second group are what we call the indirect data, the most important of which are seismic recordings. Seismic wave propagation and reflection are used to not only esti-

*Electronic address: moe@iran.usc.edu

mate, for example, the hydrocarbon content of a potential oil reservoir, but also its porosity distribution, as well as gaining insight into the spatial distributions of its fractures, faults, and strata. Since seismic records are inherently time dependent, they represent dynamic data.

In this paper we propose a different approach to the development of an optimal model of a porous formation based on the SA method. The method uses limited, but complementary, information—both static and dynamic—in order to develop the optimal model. More specifically, the aim of our work is to obtain the optimal spatial distributions of the porosity and permeability of a porous medium. In the present paper we focus on the simpler problem of determining the optimal spatial distribution of a porous formation's porosity, which is important not only to the spatial distribution and volumes of fluids that the formation contains, but also to their flow in the formation. Consistent with what happens in practice, we assume that (i) limited data are available for the porosities, in the form of porosity logs measured in certain directions (for example, along some wells) in the porous medium, and that (ii) we also have limited information on the first-arrival (FA) times of seismic waves that reach certain receivers installed in the porous medium. The waves result from a point source, or a line or plane of sources, depending on the seismic experiment. One distinct advantage of using data for the FA times in the development of the optimal model is that extensive data for the FA times are usually available for any given LS porous medium.

In order to compute the FA times, we solve the full three-dimensional (3D) wave equation which, to our knowledge, has never been attempted before in conjunction with an optimization method. An important advantage of solving the wave equation as part of the optimization process is that it is not subject to the high-frequency assumption that is essential to traditional and standard methods [17] in which the FA times are estimated by ray tracing. In addition, the method allows for any type of heterogeneities. In particular, long-range correlations, of the type that typically exist in the spatial distributions of ϕ and k [1,2,18], and the anisotropy in the form of stratification, are incorporated in the optimal model. Although various optimzation methods have been used in the past with seismic and other types of data [17,19,20], none used the full numerical simulation of the wave equation or tried to reconstruct the spatial distributions of the heterogeneities of the type that we consider. Luo and Schuster [21] did solve the 2D wave equation in order to develop a model of a porous medium based on seismic data, but their method was completely different from what we present in this paper, and was not one of optimization.

The rest of this paper is organized as follows. In Sec. II the problem that we study is described precisely. Section III presents the details of numerical simulation of the equation that describes the propagation of seismic waves in a porous medium. Section IV describes the formulation of the problem in terms of an optimization process, while Sec. V presents the details of the optimization algorithm based on the SA method. The results are presented and discussed in Sec. VI. The efficiency of the computations and how they scale with the size of the computational grid is discussed in Sec. VII, while the paper is summarized in Sec. VIII.

II. PROBLEM STATEMENT

We represent the porous medium by a computational grid of size $L_x \times L_y \times L_z$, consisting of cubic grid blocks to which the effective values of ϕ, the porosity, and $K(\phi)$, the bulk modulus, are assigned. Both ϕ and K vary spatially. In the present work we used $L_x = L_y = L_z = 15$. Larger systems can also be simulated at higher computational cost but, for the purpose of illustrating the method, the grid size that we use suffices. Consistent with what is done in practice, we assume that there are a number of wells in the porous medium, along which the porosity has been measured. More generally (particularly if one wishes to use the method for developing optimal models of laboratory-scale porous media), one may assume that estimates of the local porosities at certain points of the porous formation are available.

In the present work we assume that there are five wells in the z (vertical) direction, positioned at grid blocks $(3, 3, n)$, $(3, L_z - 2, n)$, $(L_z - 2, 3, n)$, $[(L_z + 1)/2, (L_z + 1)/2, n]$, and $(L_z - 2, L_z - 2, n)$, with, $n = 1, \ldots, L_z$. Values of ϕ for such blocks are assumed to be known and are fixed during the optimization process. However, measured data along any number of wells, or at other locations throughout the porous medium, can be used in the model. We also assume, consistent with the common practice, that as a result of having a source, seismic waves propagate throughout the porous medium, and that their first-arrival (FA) times—the time that the wave front first reaches a certain point—have been recorded by a number of receivers distributed throughout the porous medium.

The question then is, what is the optimal spatial distribution of the porosity that honors (preserves) the known values of ϕ, and reproduces as closely as possible the data for the seismic waves FA times at the receivers? To develop a method for obtaining such an optimal model, we need to be able to numerically solve the equation that governs propagation of seismic waves in a disordered porous medium. We now describe how we accomplish this.

III. NUMERICAL SIMULATION OF PROPAGATION OF SEISMIC WAVES

We model the porous formation as an elastic porous solid, and assume that the propagation of seismic waves in the formation is described by the 3D acoustic-wave equation, represented by the scalar-wave equation [22,23]. Because the porous medium is heterogeneous, its density $\rho(\mathbf{x})$ and bulk modulus $K(\mathbf{x})$ at any point $\mathbf{x}$ in the medium vary spatially. Thus, to simulate acoustic-wave propagation in such a porous medium, we solve the following equation [22,23]:

$$\frac{\partial^2}{\partial t^2} \psi(\mathbf{x}, t) - \boldsymbol{\nabla} \cdot [\lambda(\mathbf{x}) \boldsymbol{\nabla} \psi(\mathbf{x}, t)] = S(\mathbf{x}, t), \qquad (1)$$

where $\psi(\mathbf{x}, t)$ is the wave amplitude at time t (often referred to as the pressure in the geophysics literature), $\lambda(\mathbf{x}) = K(\mathbf{x})/\rho(\mathbf{x})$, and $S(\mathbf{x}, t)$ is the source function for the waves.

Before proceeding further, we must specify how the bulk modulus K depends on the porosity. Many empirical, semi-empirical, and approximate theoretical relations for $K(\phi)$

have been proposed in the past [3,4,24]. In the present work we utilize the following equation:

$$K_{dry} = K_0(1 - \phi)^{3/(1-\phi)}, \qquad (2)$$

first suggested by Krief *et al.* [25]. Here, K_{dry} and K_0 are, respectively, the bulk modulus of the dry rock and of the pure solid mineral phase. Equation (2) has been shown to be reasonably accurate in estimating the bulk modulus of a variety of porous rock. Thus, using the obvious relation, $\rho = \rho_0(1 - \phi)$, where ρ_0 is the density of the pure solid mineral phase, values of $\lambda(\mathbf{x})$ can be specified at every point $\mathbf{x}$. We emphasize that any other relation between the bulk modulus and the porosity can be used in the formulation of the problem that we describe in the present paper.

To solve Eq. (1), we use the finite-difference (FD) method with second-order discretization for the time derivative. As for the spatial derivatives, we used both second- and fourth-order discretization, but the difference between the numerical solutions obtained with the two FD discretizations was very small. Hence, using the FD approximation, we write $\psi(\mathbf{x}, t)$ as $\psi_{i,j,k}^{(n)}$, where n denotes the discrete time, and (i, j, k) represents the center of a grid block located at $\mathbf{x}$. The second-order FD approximation (accurate to Δt^2) to the time-derivative term of Eq. (1) is the standard form,

$$\frac{\partial^2 \psi(\mathbf{x}, t)}{\partial t^2} \simeq \frac{\psi_{i,j,k}^{(n+1)} - 2\psi_{i,j,k}^{(n)} + \psi_{i,j,}^{(n-1)}}{\Delta t^2}, \qquad (3)$$

where Δt is the time step's size. As for the spatial derivatives, we first expand the right side of Eq. (1) as

$$\nabla \cdot [\lambda(\mathbf{x}) \nabla \psi(\mathbf{x}, t)] = \nabla \lambda(\mathbf{x}) \cdot \nabla \psi(\mathbf{x}, t) + \lambda(\mathbf{x}) \nabla^2 \psi(\mathbf{x}, t).$$

The second-order FD approximations to the derivatives are, once again, in the standard forms. Thus, for example, $\partial^2 \psi(\mathbf{x}, t)/\partial y^2 = [\psi_{i,j+1,k}^{(n)} - 2\psi_{i,j,k}^{(n)} + \psi_{i,j-1,k}^{(n)}]/\Delta y^2$, where Δy is the linear size of the blocks in the y direction. As for the fourth-order FD discretization, we approximate, for example, the derivatives in the x direction by

$$\frac{\partial^2 \psi(\mathbf{x}, t)}{\partial x^2}$$

$$\simeq \frac{-\psi_{i+2,j,k}^{(n)} + 16\psi_{i+1,j,k}^{(n)} - 30\psi_{i,j,k}^{(n)} + 16\psi_{i-1,j,k}^{(n)} - \psi_{i-2,j,k}^{(n)}}{12\Delta x^2},$$

$$(4)$$

$$\frac{\partial \psi(\mathbf{x}, t)}{\partial x} \simeq \frac{-\psi_{i+2,j,k}^{(n)} + 8\psi_{i+1,j,k}^{(n)} - 8\psi_{i-1,j,k}^{(n)} + \psi_{i-2,j,k}^{(n)}}{12\Delta x}, \quad (5)$$

where Δx is the grid blocks' size in the x direction. Similar expressions are written down for the partial derivatives with respect to the y and the z directions. Such approximations proved to be accurate enough and provide the required stability to the numerical results [26].

To begin the simulations, we generate a pulse of waves from a source. We consider two locations for the waves' source. In one case, the source is placed at the center of the computational grid. Reflective boundary conditions are used for this case, i.e., the wave front is reflected at the bound-

aries. On the other hand, most natural porous media are anisotropic with their anisotropy caused by stratification. In a practical application of propagation of seismic waves in a porous formation for gaining information about its morphology and contents, the main direction of wave propagation may be more or less perpendicular to the planes of the strata. For example, in seismic exploration the waves' source is typically on the ground surface while the strata are more or less parallel to the ground surface. This implies that the main wave front penetrates the ground and moves perpendicular to the strata. Thus, in the second case, we place the source on the top xy plane that represents the ground surface. In this case, periodic boundary conditions are used in the x and y directions (in the horizontal planes), while the main wave front propagates in the z (vertical) direction. Such conditions do not distort the nature of the wave propagation, as we use relatively a large grid. Typically, after 500 time steps or fewer the wave front has reached all the grid blocks for the first time, although the precise number of the time steps depends on the formation's heterogeneity. As for the source function $S(\mathbf{x}, t)$, we used the following to generate the pulse of waves (any other source function may be used, however):

$$S(\mathbf{x}_s, t) = -A \exp[-\zeta(t - t_0)^2], \qquad (6)$$

where A is a constant, ζ controls the wavelength of the wave, and $\mathbf{x}_s$ is the source's location. The discretized wave equation is then solved numerically throughout the system, and the FA times for all the grid points are computed. The accuracy of the solution was checked by considering the stability criterion and the wavelength of the source [26]. The (dimensionless) time step was $\Delta t = 10^{-3}$.

IV. FORMULATION OF THE OPTIMIZATION PROBLEM

To begin the optimization process, we define, similarly to the SA method for thermal systems [15], an objective or energy function E that we seek to minimize. E is given by

$$E = W_w E_w + W_\phi E_\phi, \qquad (7)$$

where

$$E_w = \sum_{i=1}^{N_r} |t_m(i) - t_s(i)| \qquad (8)$$

is the contribution to E of the seismic data in terms of the FA times, with N_r being the number of receivers at which the FA times have been recorded. Here, $t_m(i)$ is the measured FA time at receiver i, and $t_s(i)$ the corresponding value obtained from simulation of the acoustic-wave equation described above. E_ϕ represents the contribution of the porosity data, the exact form of which depends on the data and the morphology of the porous formation. W_w and W_ϕ are the weight factors for the FA times and the porosity data, respectively. The purpose of including different weight factors in Eq. (7) is to attribute the proper importance to each component of the total energy E. Before the optimization process is begun, we should estimate the weight factors. This will be described shortly.

We have considered several types of heterogeneous porous formations which we now describe, after which the ex-

act form of E_ϕ will be given. Extensive analysis of field-scale data for the spatial distribution of the porosity indicates [1,2,18] that such data contain long-range correlations that may be described by a fractional Brownian motion (FBM), or other similar self-affine distributions. Recent works [27,28] indicate that such long-range correlations have important implications for wave propagation in large-scale porous media. Therefore, the inclusion of such long-range correlations in the optimization method proposed in the present paper, in conjunction with the acoustic-wave equation, makes the method very useful and realistic for practical applications. Thus, we assume that the porosity data along the five wells follow a FBM. However, any number of wells or, more generally, any amount of data for ϕ throughout the porous media, can be included in the model. In fact, the larger the number of the wells or the amount of data, the more accurate the optimal model would be. The two-point correlation function $C(r)$ of a FBM is given by

$$C(r) = C_1 r^{2H}, \qquad (9)$$

where $C_1 = C(r=1)$. Here, H is the Hurst exponent that characterizes the type of correlations, such that for $H > 1/2$ ($H < 1/2$) one has persistent or positive (antipersistent or negative) correlations in the successive increments of the FBM, while for $H = 1/2$ the trace of an FBM follows Brownian motion and, thus, the increments are uncorrelated. Another important property of a FBM is that its successive increments follow a Gaussian distribution (albeit with long-range correlations). Therefore, assuming that the porous formation is isotropic, and that the grid blocks' porosities in the interwell zones also follow the FBM (otherwise, there cannot be any long-range correlations in the distribution of ϕ), we have

$$E_\phi = \sum_r | \ln[C(r)] - 2H_m \ln(r) - \ln(C_1)|, \qquad (10)$$

where H_m is the Hurst exponent that one obtains (measures) from analyzing the porosity data along the wells, or any part of the porous medium for which data for ϕ are available. Equation (10) implies that the optimal porosity distribution in the interwell zones is one for which the correlation function follows Eq. (9), since no other direct data are available for such zones.

The analysis of porosity and other types of data indicates sometimes [2,18] that one should divide the zones that contain the observation wells (along which ϕ and k are measured or estimated) into subzones, each of which is characterized by a distinct H. In that case, the computational grid is also divided into similar clusters or subzones, and the sum in Eq. (10) is partitioned into several partial sums, each of which would contain a distinct H_m that represents a cluster of the wells and the part of the grid that represents that cluster.

The analysis of the porosity and other types of data may also indicate [2,18] that the extent of the correlations may be up to a distance $r = \ell$, beyond which the data become uncorrelated (ℓ is referred to as the *sill* in geostatistics [29]). Hence, for such cases the correlation function is given by

$$C(r) = \begin{cases} C_1 r^{2H}, & r \leq \ell \\ C_1 \ell^{2H}, & r > \ell, \end{cases} \qquad (11)$$

so that the energy function is given by, $E_\phi = E_r + E_\ell$, with

$$E_r = \sum_{r=1}^{\ell} |\ln[C(r)] - 2H_m \ln(r) - \ln(C_1)|, \qquad (12)$$

$$E_\ell = \sum_{r_i = \ell}^{L_n} |\ln[C(r_i)] - 2H_m \ln(\ell) - \ln(C_1)|, \qquad (13)$$

where L_n is the total distance over which the porosities in the rest of the porous medium are not correlated with the porosity data along the wells, or wherever that they have been measured or estimated. The total energy function is then given by

$$E = W_w E_w + W_r E_r + W_\ell E_\ell, \qquad (14)$$

where W_w, W_r, and W_ℓ are the corresponding weight factors (see below).

Natural porous media are almost always anisotropic, with the anisotropy caused by stratification. If the strata are more or less in the xy planes, with z representing the vertical direction perpendicular to the strata, then we have two correlation functions given by

$$C_{xy}(r) = C_1^{(xy)} r^{2H}, \quad C_z(r) = C_1^{(z)} r^{2H}. \qquad (15)$$

For such cases the energy function E_ϕ is written as $E_\phi = E_{xy} + E_z$, with

$$E_{xy} = \sum_{k=1}^{L_z} \left\{ \sum_{r_{ij}} |(\ln[C_{xy}(r_{ij}, k)] - 2H_m \ln(r_{ij}) - \ln[C_1^{(xy)}]|\right\}, \qquad (16)$$

$$E_z = \sum_{i=1}^{L_x} \sum_{j=1}^{L_y} \left\{ \sum_{r_k} |(\ln[C_z(i, j, r_k)] - 2H_m \ln(r_k) - \ln[C_1^{(z)}]|\right\}. \qquad (17)$$

The total energy function to be minimized by the SA method is then given by

$$E = W_w E_w + W_{xy} E_{xy} + W_z E_z. \qquad (18)$$

For the results that are described below, we used $C_1^{(z)}/C_1^{(xy)} = 5$. Clearly, one can also introduce cutoff length scales ℓ_{xy} and ℓ_z in the above formulation as well, which we also considered. Note that the above formulation is completely general. Any other correlation function, obtained based on the analysis of the data, can be incorporated in the above formulation. Our use of a power-law, nondecaying correlation function is not only consistent with the extensive data for many LS porous media [2,18], but also puts the model under a most stringent test of accuracy.

The weight factors introduced above must be estimated, before the actual optimization process is begun. It can be shown [30] that each weight factor is inversely proportional to the average change of its corresponding energy function,

$$W_w \propto (\langle |\Delta E_w| \rangle)^{-1}, \quad W_\phi \propto (\langle |\Delta E_\phi| \rangle)^{-1}. \quad (19)$$

In practice, the average change of each energy function cannot be computed analytically, but must be estimated numerically by evaluating the average change of, say, 10^4 independent perturbations of the system, the way it is carried out during the optimization by the SA method (see below). Typical values that we computed were $W_w \simeq 0.4$–1.6, $W_{xy} \simeq 48$–81, and $W_z \simeq 3$–4.8.

As is well known, the distributions that are to be optimized by the SA process are the result of iterating the system many times by varying the values of the quantities to be optimized. Let $B(i)$ be the value attributed to block i of the grid. After some SA iterations and changing the $B(i)$ values, there is no guarantee that, $0 < B(i) < 1$, the range in which the porosities should change. To resolve this issue, we define two parameters for each block i; $B(i)$, which is used and varied in the optimization process, and is required to follow the specified correlation function, and $\phi(i)$, the actual porosity of block i. The relation between $B(i)$ and $\phi(i)$ is given by

$$\phi(i) = \frac{B(i) - B_m}{B_M - B_m}(\phi_M - \phi_m) + \phi_m, \quad (20)$$

where ϕ_M and ϕ_m are, respectively, the maximum and minimum values of porosity that we expect the porous formation to contain (which are estimated from the porosity data and other types of geological information about the porous formation), and B_M and B_m are the corresponding values of the SA variable $B(i)$ in the entire system for every iteration.

V. THE OPTIMIZATION PROCEDURE

Having defined all the important variables and described the formulation of the problem in terms of an optimization process, we now describe the optimization procedure based on the SA method. The following computational procedure is taken in order to obtain the optimal spatial distribution of the porosity.

(1) The weight factors are estimated (see above).

(2) We distribute the $B(i)$ values in the grid blocks for which the ϕ values are not known. They are selected from a Gaussian distribution. However, any other initial distribution may be used, if need be. The corresponding porosities and bulk moduli of the blocks and, therefore, the parameter $\lambda(\mathbf{x})$ are then computed.

(3) The acoustic-wave equation is solved, and the FA times t_s are computed.

(4) The correlation function $C(r)$ of the spatial distribution of the porosities is computed. To speed up the computations, two tricks are used [31]. (i) Except for the first iteration in the optimization process, we compute the *change* in $C(r)$ between successive iterations of the SA process, not $C(r)$ itself. This reduces the simulation time very significantly. (ii) $C(r)$ is computed at selected values of $r = r_i$ with, $i = 1, m, m^2, m^3, \ldots, \frac{1}{2}N$, where N is the array's size, and $m \geqslant 1$ is an integer, instead of computing $C(r)$ at r_i with, $i = 1, 2, \ldots, N$, which also reduces the computation time significantly.

(5) The total energy function E is computed.

(6) The initial energy E_{old} is computed, and the initial "temperature" T_0 is set to be $T_0 = E_{\text{old}}$.

(7) A block i in the computational grid is selected at random, and a direction—x, or y, or z—is also chosen with equal probability. Then, the value $B(i)$ associated with the block is changed. The algorithm for doing so is [31] to change $B(i)$ to either

$$B_{\text{new}}(i) = B(i+1) + r \quad (21)$$

or

$$B_{\text{new}}(i) = B(i-1) + r, \quad (22)$$

with equal probabilities, where r is a random number selected from a Gaussian distribution with a unit variance. We found [31] this choice of r to result in accurate FBM arrays with good computational efficiency. $B(i \pm 1)$ represent the block values along the selected direction that are neighbors of the block represented by $B(i)$. Equations (21) and (22) are motivated by the fact that, as mentioned earlier, the successive increments in a FBM array follow a Gaussian distribution, and selecting r from this distribution ensures that this property is automatically built into the array. However, more generally, one may use other suitable algorithms, instead of Eqs. (21) and (22), or select the random number r from other suitable distributions, depending on the nature of the correlations.

The corresponding porosity $\phi(i)$ is then computed using Eq. (20). Note that Eqs. (21) and (22) imply that the porosity $\phi(i)$ of block i changes according to

$$\phi_{\text{new}}(i) = \phi(i+1) + r' \quad (23)$$

or

$$\phi_{\text{new}}(i) = \phi(i-1) + r', \quad (24)$$

with

$$r' = \frac{\phi_M - \phi_m}{B_M - B_m} r, \quad (25)$$

which is a rescaled Gaussian number. Equation (25) ensures that the final optimized porosity distribution will have the correct correlation function. Note also that the above scheme ensures that if the randomly selected block i lies along the wells for which porosity data are available, the value of $B(i)$ will change by the SA iteration, but $\phi(i)$ will not, hence honoring (preserving) the porosity data.

(8) The new energy, E_{new}, and the change in the energy, $\Delta E = E_{\text{new}} - E_{\text{old}}$, are computed. If $E_{\text{new}} < E_{\text{old}}$, the change is accepted and we go back to step (3) and set $E_{\text{old}} = E_{\text{new}}$. If $E_{\text{new}} > E_{\text{old}}$, the change is accepted or rejected using the Metropolis algorithm [i.e., based on a probability proportional to the Boltzmann's factor, $\exp(-\Delta E/T)$]. In any case, we go back to step (3), but keep track of the number of accepted changes. In addition, we also define and set a maximum number of iterations at each temperature, and a maximum cumulative total change in the energy. When the number of accepted energy changes reach a suitable, *a priori* specified number, or when the maximum allowed changes in the en-

ergy is reached or exceeded, step (9) described below is undertaken. Typically, at the initial steps of the SA process (at high temperatures) the accepted changes are achieved before the maximum allowed change is reached or exceeded. At very low temperatures, on the other hand, the maximum allowed changes in the energy are reached before the accepted number of changes reaches its prespecified number, as the number of rejections are large at such temperatures.

(9) The temperature is lowered according to the schedule, $T_{\text{new}} = R_T T_{\text{old}}$, where we used $R_T = 0.9$ or 0.99.

(10) We also test for convergence to the optimal system. If, for any iteration, ΔE is less than some prespecified value, the iteration is terminated. If not, the temperature is lowered according to the above schedule (after a suitable number of accepted changes is obtained, or if the maximum allowed change is reached or exceeded), and the iteration process is continued. The total number of iterations for achieving convergence depends on the system's size and the value of the Hurst exponent H. Convergence is typically reached after the maximum-allowed change in the system's energy is achieved or exceeded two or three times.

VI. RESULTS AND DISCUSSIONS

Since natural and large-scale porous media are usually stratified (anisotropic), we present the results for this type of systems, although we have also considered the case of isotropic porous media [32]. To test the accuracy of the method, we proceeded as follows. We first generated the spatial distribution of the porosities, with the statistics of a FBM and a given Hurst exponent H (with or without a cutoff length scale for the correlations; see below) and assigned them to the grid blocks, based on which we computed the corresponding blocks' bulk moduli using Eq. (2). The acoustic-wave equation was then solved numerically and the corresponding FA times at all the grid blocks were computed. We then assumed that the generated porosities along the wells, as well as the computed FA times at the receivers, represent the "data" that are then used in the optimization process (the rest of the generated porosities, as well as the computed FA times for the rest of the porous medium, are kept for comparison). The question, then, is, to what extent the optimal model reproduces the FA times at the rest of the grid blocks (*not* at the receivers), as well as the grid blocks' porosities that are *not* along the wells, or at locations where ϕ has been measured.

For the simulations described below, the number of receivers was $N_r = 156$ when we developed optimized models of stratified porous media with the waves' source being at the center. When we introduced a cutoff length scale into the correlation functions of the anisotropic media, we used $N_r = 48$ receivers. In both cases the receivers were distributed in a sphere of radius $L/2$, with $L = L_x = L_y = L_z$, centered in the middle of the computational grid. When the waves' source was on the top xy plane, the number of the receivers in the anisotropic porous media with or without a cutoff length scale for the correlations was, $N_r = 70$. In this case, the receivers were assumed to be placed along the five wells (except on the top xy surface) where the porosity data had been
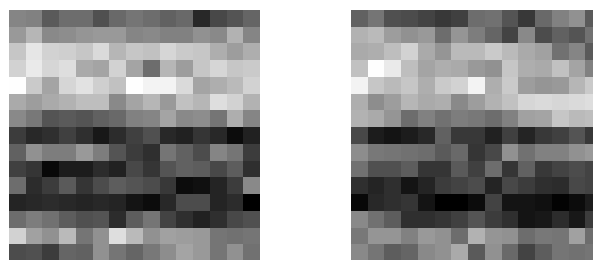
FIG. 1. The actual porosity distribution in a vertical plane at the center of the porous medium (left) and its comparison with the optimal distribution (right). Here, the Hurst exponent $H = 0.3$, and the waves' source is at the medium's center. Darkest and lightest areas show, respectively, the smallest and largest porosities.

measured. The idea is to check the model's accuracy when the number of receivers, their locations, and the positions of the seismic wave source are varied. In what follows, the results that we present for the FA times exclude those at the receivers, while the optimal porosities do not include those along the wells.

We first present and discuss the results for the case in which the wave source is at the grid's center. Figure 1 shows the spatial distribution of the porosities in a vertical plane in the middle of the medium, along with the optimal distribution that we obtained using the model. The results, which are for $H = 0.3$, indicate that the optimal distribution reproduces nicely the layered structure of the porous medium. Figure 2 presents the computed FA times in the optimal model of Fig. 1 versus the actual values. The fact that nearly all the simulated (optimal) FA times collapse onto the straight line, $Y = X$ (where they are equal to the actual values), indicates the model's accuracy. This is also indicated by the fact that the correlation coefficient R, defined by
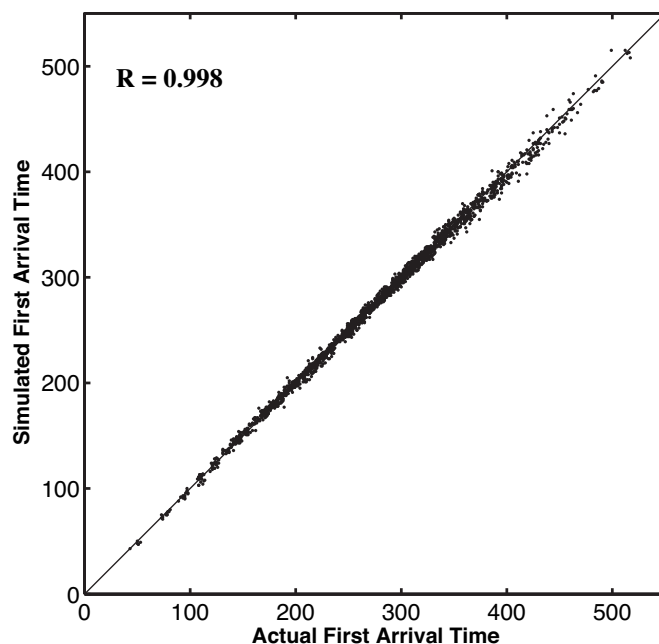
FIG. 2. Comparison of the computed (optimal) and actual first-arrival times in the porous medium of Fig. 1. R denotes the correlation coefficient.
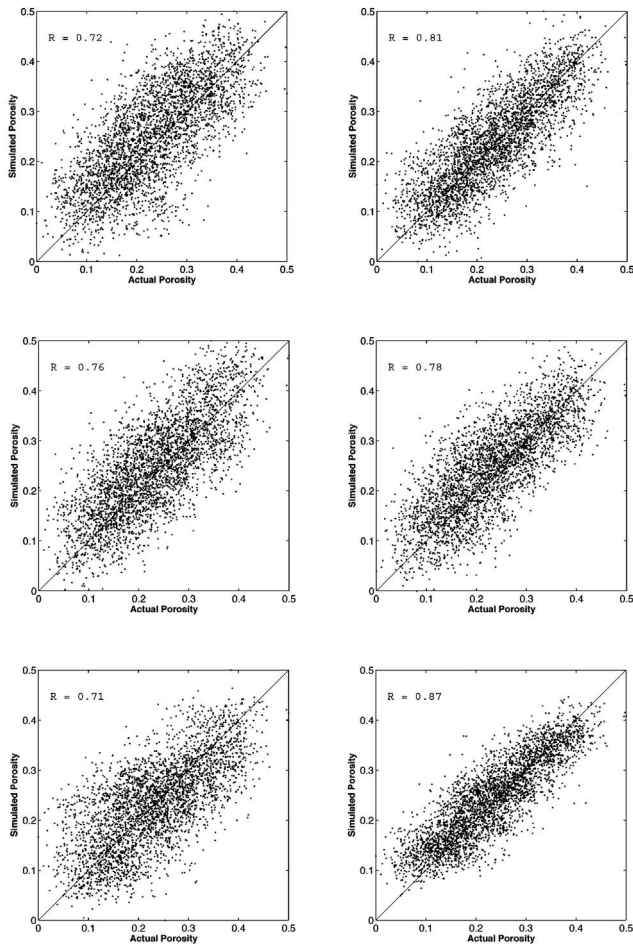
FIG. 3. Comparison of the computed (optimal) and actual porosities for 5 realizations of the porous medium of Fig. 1. The comparison with the average porosities is shown in the lowest right panel. R is the correlation coefficient.

$$R = \frac{\sum_i \left[(X_i - \langle X \rangle)(Y_i - \langle Y \rangle) \right]}{\sqrt{\sum_i (X_i - \langle X \rangle)^2 \sum_i (Y_i - \langle Y \rangle)^2}}, \qquad (26)$$

is nearly 1.0, where X_i and Y_i are, respectively, the actual (generated synthetically at the beginning) and computed optimal values of the quantity at grid block i, and $\langle X \rangle$ and $\langle Y \rangle$ are their averages. The results shown in Fig. 2 are for a single realization of the porous medium. Any other realization also has the same accuracy.

Figure 3 tests the accuracy of five realizations of porosity distribution of the porous medium of Fig. 1 (one with H =0.3). The correlation coefficient of the five realizations varies from 0.71 to 0.81, not as accurate as the computed FA times shown in Fig. 2. We must, however, keep in mind that in order to obtain the optimal porosities, we only specified their correlation function (with $H=0.3$) and the FA arrival times. The average of the five realizations (also shown in Fig. 3) is, however, much closer to the actual values, with a correlation coefficient of $R=0.87$.
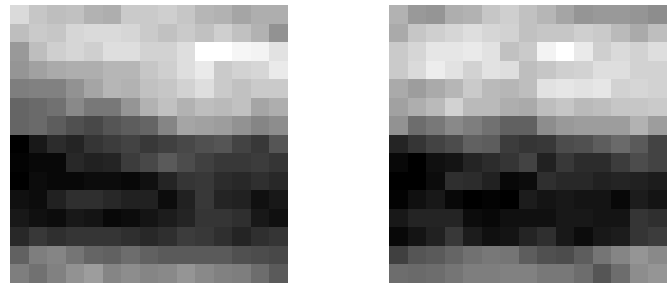
FIG. 4. Same as in Fig. 1, but for $H=0.7$. The waves' source is at the medium's center.

Figure 4 presents the actual porosity distribution for H =0.7 in a vertical plane in the middle of the porous medium and compares it with the optimal values. Once again, the optimal distribution reproduces accurately the layered structure of the medium. The corresponding FA times in the porous medium are shown in Fig. 5; the agreement between the simulated and actual values is excellent again. The accuracy of five realizations of the porous medium's computed porosities with $H=0.7$ is tested in Fig. 6, where they are compared with the actual values. In this case, the accuracy of the optimal values is good; the correlation coefficient varies between 0.91 and 0.95, with the average porosities having $R=0.96$. The reason is that $H>0.5$ corresponds to positive correlations (persistence) between the porosities, implying a much smoother porosity distribution than what one obtains with $H<0.5$. This feature enables the SA method to better locate the optimal distribution in the energy landscape. Note that the analysis of extensive data for the porosity distribution of many large-scale porous media, such as oil reservoirs around the world, indicated [2,18] that $0.7 \leqslant H \leqslant 0.8$. As Fig. 6 indi-
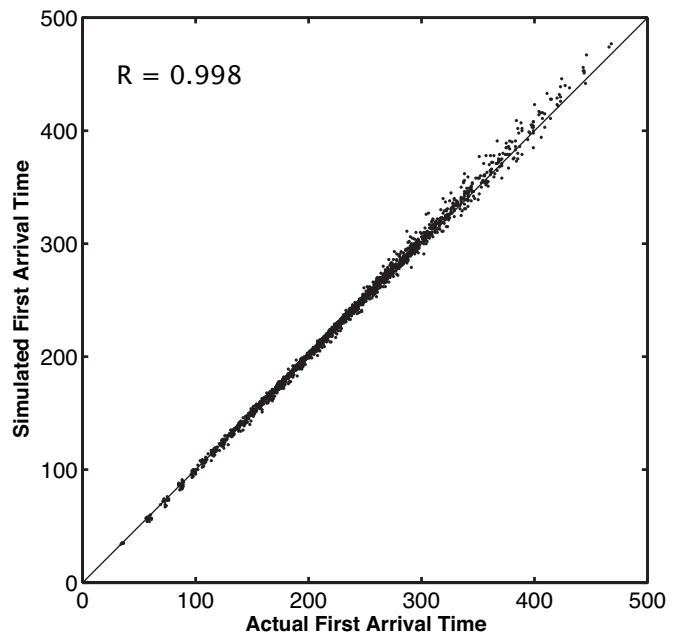
FIG. 5. Comparison of the computed and actual first-arrival times in the porous medium of Fig. 4. R is the correlation coefficient.
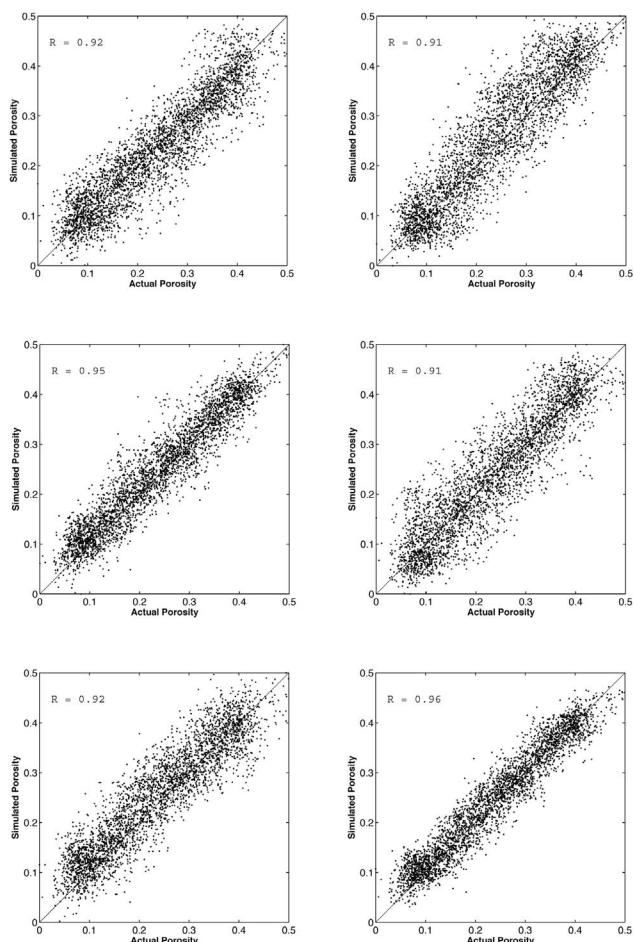
FIG. 6. Comparison of the computed and actual porosities for five realizations of the porous medium of Fig. 4. The lowest right panel shows the comparison for the average of the five realizations, with R being the correlation coefficient.

FIG. 7. Comparison of the computed and actual first-arrival times in a porous medium with $H=0.3$ and a cutoff length scale ℓ for the correlations which is one-third of the medium's linear size. The waves' source is at the medium's center.

cates, the computed optimal porosities for such values of H are particularly accurate.

We now consider another type of heterogeneity by introducing a cutoff length scale for the correlations' extent. We take the cutoff ℓ to be one-third of the medium's linear size, $\ell=\frac{1}{3}L$. Although the computed FA times, shown in Fig. 7 for $H=0.3$, are in excellent agreement with the actual values, the optimal porosities, shown in Fig. 8, are much more scattered, with a correlation coefficient R that varies between 0.69 and 0.76. The reason is that, beyond the cutoff length scale ℓ, the porosities are not correlated with one another and, therefore, may be considered as random. A random system is, however, much less constrained than a correlated one, which increases the probability that the SA method locates the actual values with less accuracy. However, similar to the case of $H>0.5$ without any cutoff length scale, the agreement between the simulated and actual values of the porosities improves when $H>0.5$. For example, Fig. 9 presents the results for $H=0.7$ and $\ell=\frac{1}{3}L$, indicating much improved accuracy (the accuracy of the computed FA times is as good as the previous cases and, hence, they are not shown).

We now present sample results for the case when the seismic-wave source is in the system's top plane, which is similar to what is practiced in application of seismic-wave propagation for exploration and obtaining data for, and insight into, the morphology of a large-scale porous medium. Figure 10 presents the actual porosities in a vertical plane in the middle of the porous medium, obtained with $H=0.3$, and compares them with the optimal distribution. Once again, all the important features of the porous medium (in particular, its strata structure) are reproduced by the optimal one. The corresponding computed FA times are shown in Fig. 11, indicating excellent agreement with the actual values. Similar to the case in which the waves' source was at the system's center, the computed (optimal) porosities are not as accurate as the corresponding FA times. This is shown in Fig. 12 for five realizations of the porosities, with the correlation coefficient varying between 0.65 and 0.74. But, when the Hurst exponent $H>0.5$, the accuracy of the results improves significantly. For example, Fig. 13 tests the accuracy of such results for 5 realizations of a porous medium with $H=0.7$. Once again, the results are reasonably accurate, with the correlation coefficient varying between 0.78 and 0.91, with that of the average porosities being 0.94. Recall, as pointed out above, that for almost all LS porous media for which the porosity data have been analyzed, $0.7 \lesssim H \lesssim 0.8$, and, as Fig. 13, indicates, the optimal porosities for such values of H are accurate.

VII. THE EFFICIENCY OF THE COMPUTATIONS

At this point we must address three important questions, namely, (i) how fast can the above computations be carried
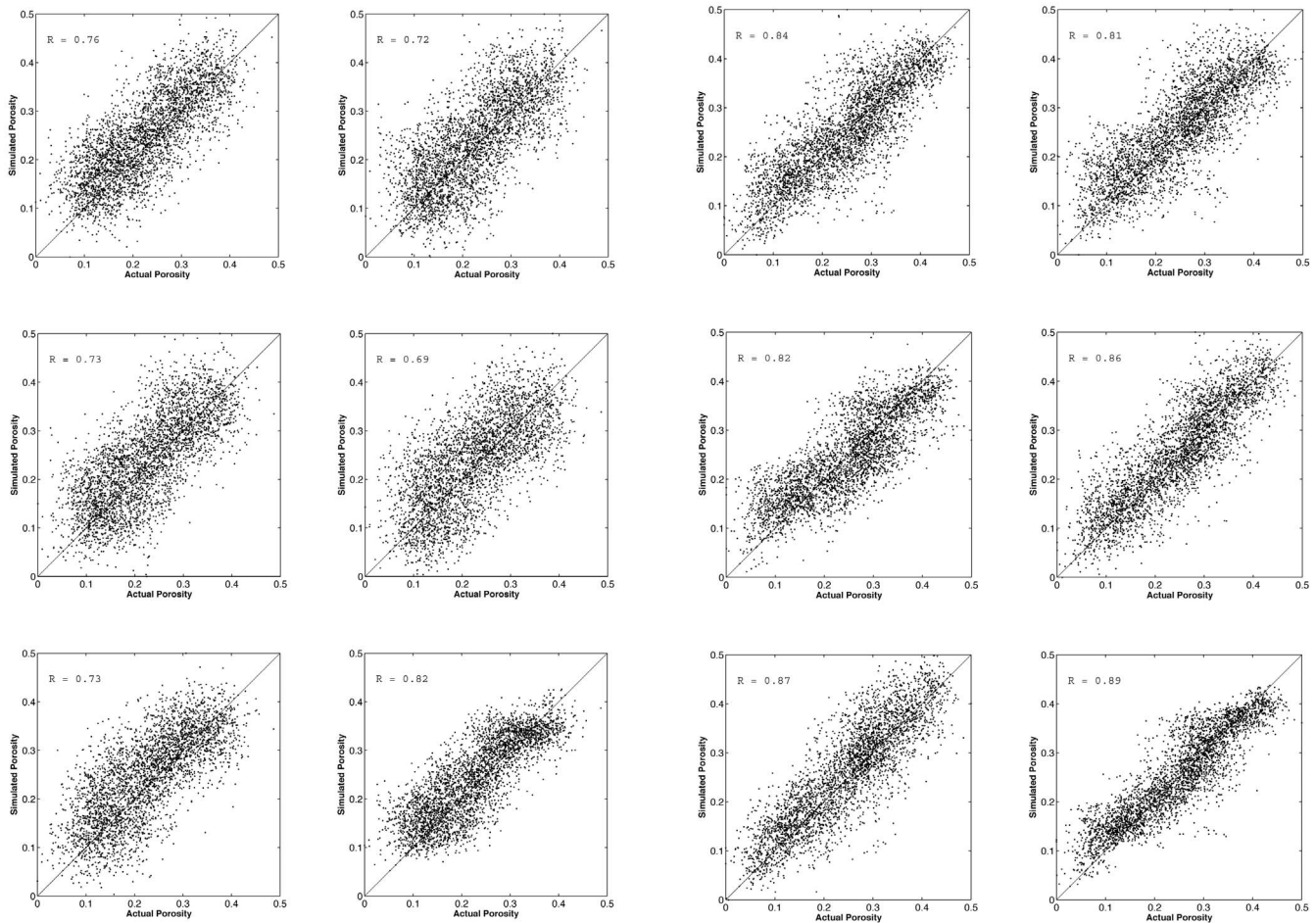
FIG. 8. Comparison of the computed and actual porosities for five realizations of the porous medium, for which the first-arrival times are shown in Fig. 7. The lowest right panel shows the comparison for the average of the five realizations.

FIG. 9. Same as in Fig. 8, but for $H=0.7$.

out? (ii) How does the computation time scale with the size of the grid representing a porous medium, or with the number of variables to be optimized, and (iii) can the optimization method developed in this paper be used in practice for modeling of large-scale porous media? To answer these questions, we consider the modeling of an oil reservoir. The size of the grid that we utilized in our computations was $15 \times 15 \times 15$. Hence, we needed to optimize the porosities of 3375 grid blocks. In practice, the geological model of an oil reservoir may contain hundreds of thousands of grid blocks. However, such a large grid is never used in the simulation of flow and transport in an oil reservoir [1,2]. Instead, the geological model is first coarsened [33], i.e., a scheme is used to create another coarser grid, beginning with the geological model, that has far fewer grid blocks of larger sizes, the effective properties of which are assigned based on those of the original geological model. Clearly, the grid that we develop by the optimization process corresponds to the coarsened or upscaled grid used in practice in the simulation of flow and transport in an oil reservoir. That this is so is due to the fact that seismic data do not have a high-enough resolution for constructing the geological model. Instead, they are

usually used for developing the spatial properties of the grid which is directly used in the simulations. The typical upscaled grid contains at most 15 000–20 000 grid blocks, which is greater than the grid that we used in our computations by a factor of about 5–6.

To estimate the computation times for a larger grid, we first point out that the times for the simulated-annealing trials and constructing the proper correlation functions for the porosities constitute a very small fraction of the total computation time. In fact, about 95% of the total computation time is spent in solving the acoustic-wave equation, Eq. (1), repeatedly after each SA trial. Thus, in what follows the estimates
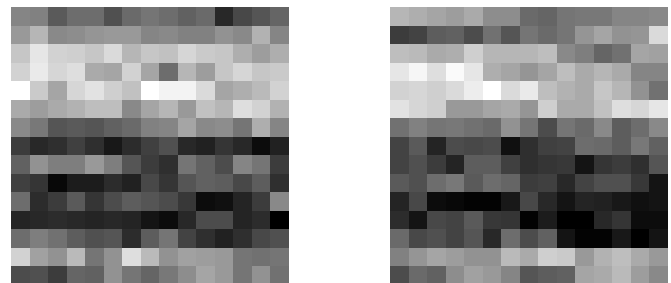
FIG. 10. Same as in Fig. 1 ($H=0.3$), but with the waves' source in the top plane of the medium.
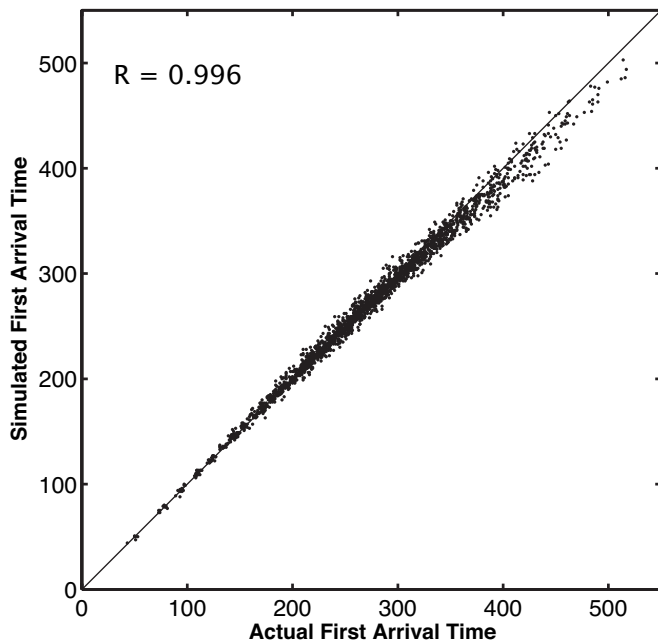
FIG. 11. Comparison of the computed and actual first-arrival times in the porous medium of Fig. 10.

that we present are based on the computation times for solving Eq. (1) in a large grid. To estimate the computation times, we consider the calculations on, (i) a *single* fast computer, and (ii) a parallel machine with many nodes and processors.

A. Computations using a single workstation

The total computation times for the grid that we used in our calculation is about 3.2 CPU days on a Pentium 4 (P4) machine at 3.8 GHz (the fastest P4 machine currently available). Use of SUN AMD Opteron workstations reduces the computations by at least 25%, which means the computations for the grid size that we used will further reduce to about 2.4 CPU days on such workstations. Since, as pointed out above, the computations are dominated by the time used for solving the acoustic-wave equation repeatedly during the SA iterations, we need to know how the times for computing this solution scales with the grid size. Since we use a fully explicit finite-difference approximation for discretizing the acoustic-wave equation, obtaining its numerical solution does not involve any iterative scheme. Instead, one "marches" forward, starting from the grid points around the wave source, and computes the waves' amplitudes ψ grid point by grid point. Under these conditions, the computation times for solving the acoustic-wave equation scales linearly with the grid size. Therefore, for a grid that contains about 20 000 blocks, the computation time for developing its optimal porosity distribution will be on the order of 15 CPU days on a dedicated workstation, completely acceptable and practicable with the currently available SUN workstations (even with a P4 machine the computations will take on the order of 20 CPU days, which is still acceptable). Note that such machines can have up to six processors and, therefore, the
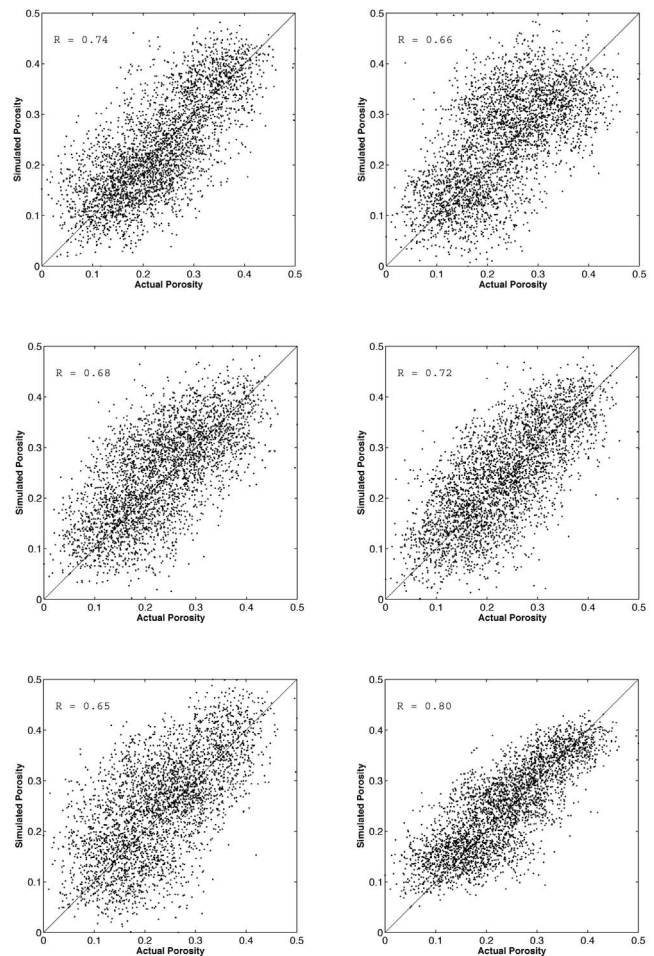
FIG. 12. Comparison of the computed and actual porosities for five realizations of the porous medium of Fig. 10 ($H=0.3$), in which the waves' source is in the medium's top plane. The lowest right panel shows the comparison for the average of the five realizations.

computation time can be further reduced significantly.

We also point out that we have made no attempt to optimize the method that we use for obtaining the numerical solution of the acoustic-wave equation. If this is done, the optimization process will be carried out more efficiently. Consider, for example, the fact that after each SA iteration, we change the porosity of only a single block. The rest of the porosities remain intact. Therefore, the solutions of the wave equation in the grid, before and after changing the porosity of a single block, do not differ significantly in most of the grid; they only differ slightly around the block where the porosity is altered by the SA method. This is particularly true when the grid size is very large, on the order of the size used in the modeling and simulation of oil reservoirs. One should be able to take advantage of this fact and develop a scheme whereby, after each SA iteration, the waves' amplitudes at only a fraction of the grid blocks (around the block the porosity of which is altered by the SA method) are updated, with the rest remaining intact. This aspect is currently under study.
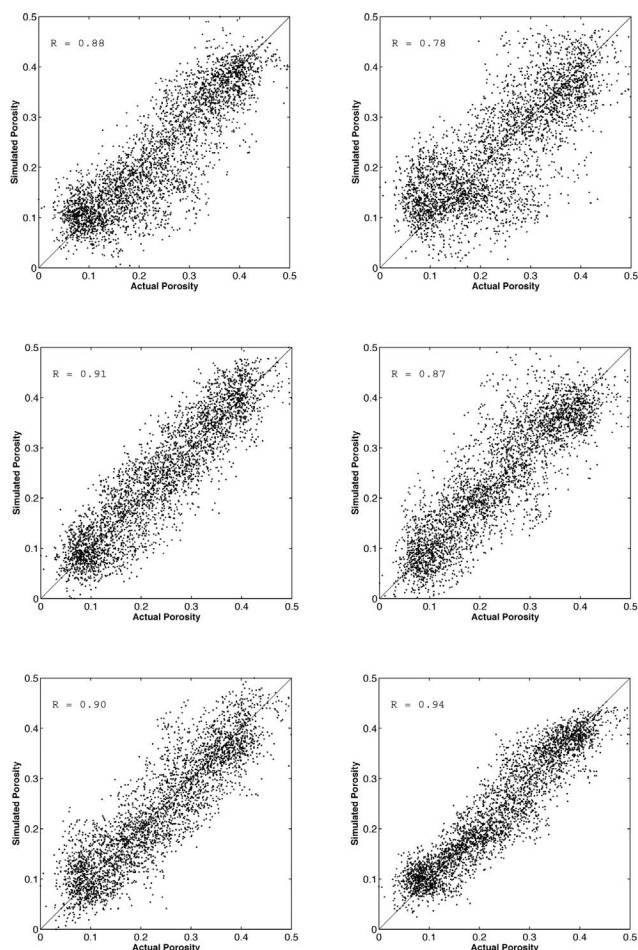
FIG. 13. Same as in Fig. 12, but for $H = 0.7$.

B. Computations with parallel computers

If a computational grid is desired that must have a number of blocks much larger than the 20 000 that we based our estimates on, then one should resort to parallel computations. Fast algorithms have already been developed for numerical simulation of the acoustic-wave equation [34] and its generalization to nonlinear and vector (elastic) wave equations [35], if the equations are discretized by the FD approximation. In these algorithms parallelization is based on the domain decomposition method, and the communications between the nodes are performed by using the message-passing interface (MPI) strategy. These algorithms have a speed up of at least one order of magnitude. When they are used on massively parallel machines, their performance is excellent, even for grids as large as 500^3 [35]. Given that, as we pointed out above, determining the numerical solution of the wave equation takes nearly 95% of the total computation time in the optimization method, these algorithms greatly facilitate the use of grids that are much larger than what we are discussing here.

Although the SA part of the method that we propose in this paper takes a small fraction of the total computation time, one must also have a parallel computational strategy for the annealing part, in order to be able to use efficiently the parallel algorithm for the solution of the wave equation. Parallel strategies have been developed for the SA method [36] with large speed up and high efficiency. Hence, one can develop an integrated parallel computational strategy for the optimization method that we propose in this paper, and carry out simulations with large grids. We have already carried out [37] such computations for a problem somewhat similar to what we describe in the present paper, namely, development of the optimal spatial distributions of the permeabilities and porosities for a large-scale porous medium in which four different gases flow and react with each other. The computations for this problem are even more intensive than what we consider in the present paper, as one must solve [38] the convection-diffusion-reaction equation [1,2] for each component, where the reactions typically follow nonlinear kinetics. In addition to the permeabilities and porosities, we have been able to optimize [37] the spatial distribution of the reaction rates of the four gases. Using a parallel computational algorithm with the MPI strategy, we have been able to develop the optimal spatial distributions of the permeabilities, porosities, and the reaction rates in a model porous medium with tens of thousands of grid blocks.

VIII. SUMMARY

We assumed that propagation of seismic waves in a large-scale porous medium is described by the acoustic-wave equation. We showed that (1) if an efficient numerical simulator that solves the acoustic-wave equation and provides estimates of the first-arrival times of the waves at a certain number of receivers scattered throughout a large-scale porous medium is incorporated in (2) a simulator that utilizes the simulated-annealing method and limited data for the FA times and the porosities of the porous medium, one obtains an optimal spatial distribution of the porosities that not only honors (preserves) the limited data, but also is accurate. We demonstrated this for several illustrative examples in which the wave source was either at the center of the porous medium or, as is commonly practiced, at its top. The formulation is completely general, and is applicable to any type of correlation function that the porosity data may follow.

There are several ways by which one can still improve the accuracy of the method. Clearly, the more data are available, the more constrained, and hence the more accurate, is the optimal model. In fact, we shall show in a future publication that incorporation of a limited amount of dynamic (time-dependent) data for fluid flow in a porous medium in the model that we described in this paper will not only result in an improved spatial distribution of the porosities, but also yield an accurate spatial distribution of the permeabilities of the porous medium. In addition, we shall demonstrate that the optimal model so obtained can provide accurate predictions for the future behavior of the porous medium, and, in particular, its flow properties.

Another way by which one can improve the model is the use of the elastic-wave equation that supports propagation of both the P and S waves (the acoustic-wave equation can describe only the propagation of the P waves). This would, of course, entail much more intensive computations. Finally,

the use of larger computational grids, which would reduce, or eliminate altogether, the effect of porous medium boundaries (which do affect the solution of the wave equation), should improve the model's accuracy. These aspects will be taken up in our future papers.

[1] P. M. Adler, *Porous Media: Geometry and Transport* (Butterworth-Heinemann, Boston, 1992); P. M. Adler and J.-F. Thovert, *Fractures and Fracture Networks* (Kluwer, Dordrecht, 1999).

[2] M. Sahimi, Rev. Mod. Phys. **65**, 1393 (1993); *Flow and Transport in Porous Media and Fractured Rock* (VCH, Weinheim, Germany, 1995).

[3] S. Torquato, *Random Heterogeneous Materials* (Springer, New York, 2002).

[4] M. Sahimi, *Heterogeneous Materials I* (Springer, New York, 2003).

[5] J. W. Cahn, J. Chem. Phys. **42**, 93 (1965).

[6] M. Joshi, Ph.D. thesis, University of Kansas, Lawrence, 1974 (unpublished).

[7] J. A. Quiblier, J. Colloid Interface Sci. **98**, 84 (1984).

[8] P. M. Adler, C. G. Jacquin, and J. A. Quiblier, Int. J. Multiphase Flow **16**, 691 (1990); P. M. Adler, C. G. Jacquin, and J. F. Thovert, Water Resour. Res. **28**, 1571 (1992); J. Poutet, D. Manzoni, F. Hage-Chehade, C. G. Jacquin, M. J. Boutéca, J. F. Thovert, and P. M. Adler, Int. J. Rock Mech. Min. Sci. Geomech. Abstr. **33**, 409 (1996); J.-F. Thovert, F. Yousefian, P. Spanne, C. G. Jacquin, and P. M. Adler, Phys. Rev. E **63**, 061307 (2001).

[9] N. F. Berk, Phys. Rev. Lett. **58**, 2718 (1987); Phys. Rev. A **44**, 5069 (1991).

[10] M. Teubner, Europhys. Lett. **14**, 403 (1991).

[11] A. P. Roberts and M. Teubner, Phys. Rev. E **51**, 4141 (1995); A. P. Roberts and M. A. Knackstedt, *ibid.* **54**, 2313 (1996).

[12] M. D. Rintoul and S. Torquato, J. Colloid Interface Sci. **186**, 467 (1997).

[13] C. L. Y. Yeong and S. Torquato, Phys. Rev. E **57**, 495 (1997); **58**, 224 (1998).

[14] C. Manwart, S. Torquato, and R. Hilfer, Phys. Rev. E **62**, 893 (2000).

[15] S. Kirkpatrick, C. D. Gellat, Jr., and M. P. Vecchi, Science **220**, 671 (1983).

[16] R. W. Mair, G. P. Wong, D. Hoffmann, M. D. Hürlimann, S. Patz, L. M. Schwartz, and R. L. Walsworth, Phys. Rev. Lett. **83**, 3324 (1999).

[17] See, for example, M. Sen and P. L. Stoffa, *Global Optimization Methods in Geophysical Inversion* (Elsevier, Amsterdam, 1995).

[18] H. H. Hardy and R. A. Beier, *Fractals in Reservoir Engineering* (World Scientific, Singapore, 1994).

[19] M. K. Sen and P. L. Stoffa, Geophysics **56**, 1624 (1991); X.-Q. Ma, *ibid.* **67**, 1877 (2000); K. P. Dorrington and C. A. Link, *ibid.* **69**, 212 (2004); M. Bosch, *ibid.* **69**, 1272 (2004).

[20] C. E. Romero and J. N. Carter, J. Pet. Sci. Eng. **31**, 113 (2001).

[21] Y. Luo and G. T. Schuster, Geophysics **56**, 645 (1991).

[22] D. Sornette, Acustica **67**, 199 (1989); **67**, 251 (1989); **68**, 15 (1989).

[23] A. Ishimaru, *Wave Propagation and Scattering in Random Media* (Oxford University Press, Oxford, England, 1997); N. Bleistein, J. K. Cohen, and J. W. Stockwell, Jr., *Mathematics of Multidimensional Seismic Imaging, Migration, and Inversion* (Springer, New York, 2001).

[24] M. A. Knackstedt, C. H. Arns, and W. V. Pinczewski, Geophysics **68**, 1822 (2003).

[25] M. Krief, J. Garat, J. Stellingwerff, and J. Ventre, Log Analyst **31**, 355 (1990).

[26] M. A. Dablain, Geophysics **51**, 54 (1986); G. Kneib and C. Kerner, *ibid.* **58**, 576 (1993).

[27] F. Shahbazi, A. Bahraminasab, S. M. Vaez Allaei, M. Sahimi, and M. R. Rahimi Tabar, Phys. Rev. Lett. **94**, 165505 (2005); A. Bahraminasab, S. M. Vaez Allaei, F. Shahbazi, M. Sahimi, and M. R. Rahimi Tabar, Phys. Rev. B (to be published).

[28] M. Sahimi and S. E. Tajer, Phys. Rev. E **71**, 046301 (2005); S. M. Vaez Allaei and M. Sahimi, Phys. Rev. Lett. **96**, 075507 (2006).

[29] J. L. Jensen, L. W. Lake, P. W. M. Corbett, and D. J. Goggin, *Statistics for Petroleum Engineers and Geoscientists*, 2nd ed. (Elsevier, Amsterdam, 2000).

[30] C. V. Deutsch and A. G. Journel, *Geostatistical Software Library and User's Guide*, 2nd ed. (Oxford University Press, New York, 1998).

[31] H. Hamzehpour and M. Sahimi, Phys. Rev. E **73**, 056121 (2006).

[32] H. Hamzehpour, Ph.D. thesis, Institute for Advanced Studies in Basic Sciences, Zanjan, Iran, 2006 (unpublished).

[33] F. Ebrahimi and M. Sahimi, Transp. Porous Media **57**, 75 (2004).

[34] X. Cai and A. Odegard, in Proceedings of the 2nd IEEE International Conference on Cluster Computing, Germany, 2000 (unpublished), p. 185; T. Bohlen, Comput. Geosci. **28**, 887 (2002).

[35] S. Phadke, D. Bhardwaj, and S. Yerneni, in Proceedings of the Conference and Exposition on Petroleum Geophysics, San Antonio, Texas, 2000, Society of Petroleum Geologists (SPG 2000) (unpublished), p. 168; N. L. Armstrong-Crews, in Proceedings of the International Conference on Parallel and Distributed Processing Techniques and Applications, Houston, Texas (PDPTA) 2003 (unpublished), p. 1946.

[36] D. R. Greening, Physica D **42**, 293 (1990); D. Janaki Ram, T. H. Sreenivas, and K. Ganapathy, J. Parallel Distrib. Comput. **37**, 207 (1996); C. Meise, Stochastic Proc. Appl. **76**, 99 (1998); J. P. B. Leite and B. H. V. Topping, Comput. Struct. **73**, 545 (1999); A. Bevilacqua, J. Parallel Distrib. Comput. **62**, 1548 (2002); H. Ye and Z. Lin, Eur. J. Oper. Res. **173**, 59 (2006).

[37] R. Sanchez, T. T. Tsotsis, and M. Sahimi, Chem. Eng. Sci. (to be published).

[38] R. Sanchez, M. Hashemi, T. T. Tsotsis, and M. Sahimi, Chem. Eng. Sci. **61**, 4750 (2006).